

SIR-C MODAL SURVEY: A CASE STUDY IN FREE-FREE TESTING

Kenneth S. Smith and Chia-Yen Peng

Applied Mechanics Technologies Section
Structures and Dynamics Research Group
Jet Propulsion Laboratory
California Institute of Technology
Pasadena, California 91109

ABSTRACT

There has been an increased interest recently in developing alternatives to fixed-base modal testing for verification of large Space Shuttle payloads. A promising approach is free-free modal testing, augmented with residual flexibility measurements obtained from interface verification testing. This paper presents summary results from the recent free-free test performed on the Shuttle Imaging Radar-C payload. The test presented special challenges, both experimental and analytical. Some of the lessons learned through this effort are summarized.

1. INTRODUCTION

Dynamic model verification for large, across-the-bay Space Shuttle payloads poses a challenge for payload developers. In order to provide the proper boundary conditions at the interface to the Shuttle orbiter, a sizeable investment is required to develop and qualify a test fixture. Ref. [1] discusses one such effort. The costs involved are prohibitive unless spread over a number of payload development programs. And even in well-planned programs, it is not easy to overcome interactions between test fixture and test article, which makes test data interpretation problematic. The difficulty of fixed-base testing increases with the size and weight of the payload.

Considerable interest and research has recently been directed toward development of lower cost alternatives to fixed-base testing [2,3,4]. Particular attention has been given to variations of free-free modal testing, in which the test article is not constrained at the orbiter interface. It has been recognized that the free-free modes themselves do not contain sufficient information to verify the properties of the interface structure, so the free-free modal data must be augmented with some form of interface verification testing. Alternatives such as mass-loading of the interface or measurement of residual flexibility have been proposed.

This paper describes a recent application of free-free testing with residual flexibility measurement. The test was performed on a large across-the-bay Space Shuttle payload, the Shuttle Imaging Radar-C [5].

2. TEST ARTICLE

The Shuttle Imaging Radar-C (SIR-C) is an imaging radar system scheduled for launch aboard the Space Shuttle in 1994 (Fig. 1). The SIR-C antenna is the largest (12 meters by 4 meters) and most massive (10,500 kg) piece of flight hardware ever assembled at the Jet Propulsion Laboratory (JPL) for NASA. When it rides aboard the space shuttle, it will fill nearly the entire cargo bay.

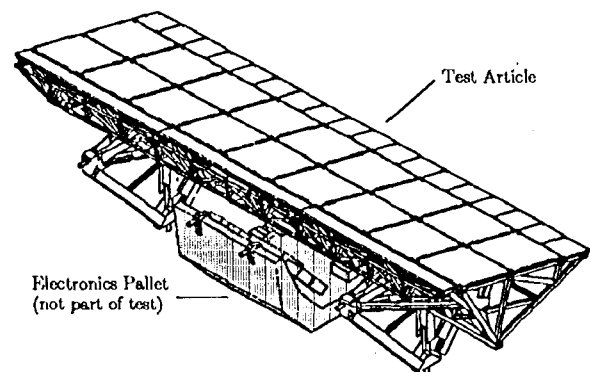


Figure 1. SIR-C Antenna Mechanical System

The SIR-C payload attaches to the orbiter via six trunnions—two sill trunnions and one keel trunnion at each of two longitudinal stations. The distance between forward and aft trunnions is 7.2 meters. Development of a fixture for fixed-base testing of this payload was not considered feasible, so free-free testing was a desirable alternative.

An unusual feature of the test article is the large number of load-carrying interface degrees of freedom. Each of the six trunnions attaches to the orbiter in two translational degrees of freedom, for a total of 12 attachment degrees of freedom. The redundancy of this interface is relieved by mechanisms within the structure, so that thermal expansion does not distort the antenna. As a result, when the structure is free-free, there are 5 low-frequency mechanism modes in addition to the usual 6 rigid body modes. These mechanism modes are well understood from the geometry of the structure, as are the rigid body modes.

When fixed at the orbiter attachment degrees of freedom, the lowest natural frequency of the SIR-C payload is 11.5 Hz. The lowest free-free mode of the payload, after the rigid body and mechanism modes, has a natural frequency of 7.5 Hz.

3. GENERAL APPROACH TO FREE-FREE TESTING

The most widely accepted practice for Shuttle payload model verification is through a fixed-base modal survey. (Fixed-base means that the degrees of freedom which will carry loads to the orbiter are grounded in the test.) One reason for doing fixed-base testing is that the model as delivered is described in terms of fixed-base modes. However, this is only a mathematical convenience, and the identical model could be described in terms of free-free or mass-loaded modes, or in many other ways, and all of these mathematical approaches would lead to exactly the same predicted loads. In fact, the only rational criteria for selecting one test method over another is not the nature of the mathematical formulation, but rather how closely the test-measured modes approximate the actual modes which will be exercised during flight.

Of course, the actual in-flight modes are not the fixed-base modes, either, because the Shuttle orbiter is not a rigid or infinitely massive structure. In fact, the dynamic mass of the orbiter is not significantly greater than that of many payloads in the frequency range of payload resonances. It is generally assumed, however, that the coupled system mode shapes in the payload tend to resemble fixed-base component modes more closely than free-free or mass-loaded component modes. Probably this assumption needs to be questioned, particularly for stiff payloads.

Having stated some concerns about a predisposition toward fixed-base tests in all cases, we nevertheless realize that there is a long heritage of using fixed-base tests to verify space payloads. As a result, we accept for now that our goal is to get acceptable agreement between the modeled and the actual fixed-base modes of the payload. This leads to well-defined test criteria, but places perhaps overly stringent requirements on the use of free-free test data. Ideally, one would like to demonstrate agreement of true flight modes, which are neither fixed nor free, but no one has yet shown how to do this.

Given that we must show verification of the fixed-base modes, the approach for using free-free modal data to satisfy this requirement is as follows. The free-free modes and residual

flexibility of the structure are measured, and the finite element model is updated to agree with the test results. A mathematical representation of the payload is now developed using only test-verified free-free modes and residual flexibility. Each of the modes of this representation will have been test-verified, so the free-free modal model can be considered test-verified. But it remains to show that this representation contains enough free-free modes to accurately predict the significant fixed-base modes of the payload. The fixed-base modes of the payload are computed using both the full model and the free-free modal representation, containing only the test-verified free-free modes. If the two resulting sets of fixed-base mode shapes and frequencies agree, then the free-free modal model is just a different mathematical representation for a test-verified fixed-base modal model.

4. EXPERIMENTAL METHODS

For programmatic reasons, the modal test was performed in two phases. In phase 1, only the core structure was present, and the radar panels were simulated with rigid mass dummies. In the phase 2, representative panels were included.

The test article was suspended at the four sill trunnions from gantries, through four airbag isolation systems (see Figures 2 and 3). Based on pre-test analysis, the highest of the 11 suspension modes (6 rigid body plus 5 internal mechanism modes) was predicted before the test to be 2.8 Hz, while the lowest free-free mode was predicted to be above 9 Hz.

The structure was instrumented with a total of 273 PCB Structural accelerometers, 28 of which were on the airbags and suspension cables. (In the phase 1 configuration, only 178 accelerometers were needed.) The instrumented locations were selected based on several criteria, including a requirement that sufficient measurements be taken such that Guyan mass matrix reduction is acceptable. The full set of measurements, including repeat cross measurements of drive point force and acceleration, was acquired in 5 banks of 80 channels each, using a Zonic Workstation 70Q0 data acquisition computer.

The accelerometers were tracked during calibration and installation with a bar code scheme, which proved invaluable both in speeding up the installation process and in preventing keypunching or other errors.

Burst random excitation was applied by up to four 445N (100 pound) VTS-100 shakers (Fig. 4). The random excitation was band limited to roll off below 8 Hz and above 60 Hz. During phase 1 of the test, all 12 of the orbiter interface degrees of freedom were driven directly by shakers, providing direct measurements of frequency response functions (FRF's). In addition to free-free modal parameter estimation, the FRF data was necessary for later extraction of residual flexibility associated with each of the interface degrees of freedom. Shakers were also placed at key locations internal to the structure to provide better data on key modes. In the second

phase of the test, only four of the 12 interface degrees of freedom were driven, due to time constraints.

Response data was acquired at multiple force levels, and critical modes were also acquired with sinusoidal excitation at increasing force levels. This approach allowed a systematic investigation of nonlinearities.

Exhaustive checks of coherence and reciprocity were performed during data acquisition.

5. FREE-FREE MODE EXTRACTION

Following measurement of FRF's, modal parameters (frequency, damping, mode shape) of the free-free modes were extracted with the polyreference time domain method, using SDRC I-DEAS. Multiple measurements of the same mode in different runs were identified by orthogonality calculations. Modes of the suspension system were identified based on kinetic energy, and were eliminated from the set. A total of 44 distinct structural modes were finally retained in each of the two test configurations, in the frequency range from 5 to 60 Hz. The frequencies of the first 11 modes from phase 1, and the first 9 from phase 2, are listed on the left side of Tables 3 and 4.

The quality of the experimental modes was assessed primarily by computing orthogonality of the test modes using the Guyan reduced analytical mass matrix (Tables 1 and 2). One or two of the test modes failed the orthogonality criterion in phase 1. The phase 2 test modes did not exhibit the same orthogonality problem. The large self-orthogonality numbers in phase 1 were attributed to structural nonlinearity associated with several closely coupled modes from 17 to 22 Hz. Either the nonlinearity or the degree of coupling was apparently reduced in the phase 2 configuration. For this reason, the phase 2 test results are considered more reliable.

It was recognized during the test that the airbag suspension system added significant mass (170 kg) to the trunnions in the vertical direction. When this mass was added to the model, the first elastic free-free mode dropped from 9 Hz to below 8 Hz, and agreed closely with the test measurements.

6. RESIDUAL FLEXIBILITY EXTRACTION

A critical requirement of the test was that residual flexibility be extracted from the measured FRF's. The combination of free-free and residual flexibility shapes is analogous to the combination of fixed-base and constraint modes in providing a statically complete representation of structural motions.

Residual flexibility is a summation over high frequency modes of the modal flexibilities. The residual flexibility value depends on which modes are included in the sum. The residual flexibility of high frequency modes appears in low frequency acceleration/force FRF's as a term proportional to frequency squared. This term is combined in the data with resonance

peaks due to low frequency modes, and with a constant (inertance) term due to rigid body and mechanism modes, as illustrated in Fig. 5. The residual flexibility is revealed by subtracting from the FRF the inertance and the resonant terms. Therefore its accuracy is dependent on the accuracy with which the inertance and modal terms are estimated and subtracted.

We discovered that it was very difficult to extract residual flexibility from the test data. If one subtracts all curve-fit modes in order to expose the residual flexibility from unmeasured high frequency modes, all of the errors of the curve-fit modes add to the error of the residual flexibility estimate. When there are many overlapping modes, the errors are amplified by resonance effects, making it doubly difficult to extract accurate residual flexibilities.

The approach we followed for the SIR-C test was to subtract only the first few elastic modes from the FRF (described as mid frequency modes in Fig. 5), since these were known very accurately. The underlying flexibility line then defined the residual flexibility summed over the remaining modes, including many other curve-fit modes. Comparisons between test and analysis residual flexibility were made based on this measurement of residual flexibility. In order to estimate residual flexibility for only the unmeasured modes, the test-derived modal flexibilities for the intermediate curve-fit modes could be subtracted numerically.

The process is illustrated by Figures 6 through 9. Fig. 6 shows a representative drive point FRF. The mode at 7.8 Hz was very accurately known. Fig. 7 shows the curve fit for that mode overlaid on the test data. After subtracting this curve-fit mode from the FRF, Fig. 8 is obtained. In the low frequency range, the remaining FRF can be approximated as the sum of a constant inertance and a residual flexibility term proportional to frequency squared. The inertance term is known based on the measured mass properties of the structure. This constant was subtracted from the FRF, and the result divided by W^2 , resulting in Fig. 9. In this figure, it can be seen that between 10 Hz and 15 Hz, the function is nearly constant. The value of this constant, which had multiplied ω^2 in the original FRF, is the estimate of the residual flexibility. Note that this measurement of residual flexibility is summed over all modes higher than the 7.8 Hz mode.

This approach was not without its own difficulties. At lower frequencies, the inertance term from rigid body modes tends to be large in proportion to the residual flexibility term. Therefore, any errors in subtracting out the inertance term result in errors in the residual flexibility estimate. Another difficulty encountered with some FRF's was the effect of nonlinearity, which made it impossible to account for the FRF with linear modal curve-fitting.

One of the most problematical aspects of residual flexibility estimation is that there are few checks which can be performed. When estimating mode shapes, it is usually apparent from mode shape plots if the data looks reasonable. In the case of residual flexibility, we know of no such sanity checks for the

*estimates. As a result, it is possible for large undetected errors to be present in the data. The only sanity check we were able to devise was to check the flatness of the curves such as Fig. 9.

7. MODEL CORRELATION

Updates to the finite element model were required to improve agreement with the test data. The major correlation effort was focused on the free-free modes. Some large errors in the model were apparent, and these were manually corrected. Further refinement was performed using structural parameter based model updating. A large number of structural parameters (bar areas and inertias, etc.) were identified as candidates for adjustment. These parameters were iteratively adjusted based on linear sensitivity calculations for both frequency and cross orthogonality. The technique described in [6] allowed many iterations to be performed almost in real time. Parameter adjustments were selected which provided the best improvement in test/analysis agreement, while at the same time minimizing the percent change in the parameters. This effort successfully produced a single set of parameters such that the model was able to match modes measured in both phases of the test. The parameter adjustments were checked for reasonableness, and all changes were justifiable.

Tables 3 and 4 show comparisons of natural frequencies between test and the post-correlation analysis model (referred to as TAM26). Tables 5 and 6 show cross orthogonality computed between the test and analysis mode shapes.

In phase 1, three of the modes failed the original goal of 5% frequency agreement, and a number of large off-diagonal cross orthogonality terms remained after correlation. It should be noted that the 5.7 Hz mode is actually a mechanism mode which will be restrained when the payload is installed in the orbiter. Therefore its stiffness is not significant. Test mode 3 (17.50 Hz) was considered suspect due to the poor self-orthogonality results, so the model was not forced into agreement.

The phase 2 correlation results are better than the phase 1 results. (This is fortunate, since the phase 2 configuration is the flight-like configuration. In fact, the model updating process was weighted toward obtaining good phase 2 agreement.) The 5% frequency match goal was attained for all modes except the first, which is not significant to the fixed-base modes. Cross orthogonality shows fairly good mode shape agreement. The only significant concern with the phase 2 results is that analysis mode 15 (15.89 Hz) was not measured during the test. It was concluded that this is a valid mode, which was not excited by the shaker locations in the phase 2 test. Therefore this mode is not considered test-verified.

After correlation of the model to the free-free modes, the residual flexibility from analysis was compared to the test measurements, which had been extracted as described in section 6. Residual flexibility was only available in the phase 1

configuration, but the phase 2 data was also checked to assure that the flexibility measurements were consistent with phase 1.

Table 7 shows a comparison of the diagonal (drive point) residual flexibility extracted from test data vs. the analytical model predictions. The flexibilities in the table are summed over all modes above 15 Hz. Note that the analysis model uniformly underpredicts the residual flexibility, by about 25%. There are a couple of terms where the analysis flexibility prediction is less than 50% of the measurement, but on closer examination the test data was considered of poor quality. Our observation is that test errors have a systematic tendency to increase the estimate of residual flexibility. It is unclear whether the analytical model is overly stiff, or whether the test results are skewed toward overestimates of residual flexibility.

No model updating was performed to improve the residual flexibility agreement between test and analysis for the SIR-C payload. Some effort was expended to determine the influence of the residual flexibility terms on the fixed-base mode predictions. It was estimated that the differences seen in Table 7 could result in fixed-base frequency differences of up to 10%. Because we did not have full confidence in the measured residual flexibility, and because the model did not agree with test measurements, this 10% uncertainty in frequency remains in the final dynamic model.

8. VERIFICATION OF FIXED-BASE MODES

The stated goal of the test was to demonstrate that the significant fixed-base modes of the structure were verified. Since the fixed-base modes were never measured directly, an indirect approach as described in [5] and [7] was used. The idea is to establish an equivalence between the representation of the structure in terms of free-free modes with residual flexibility and its representation in terms of fixed-base modes. This equivalence is demonstrated by using the free-free modal model to predict fixed-base mode frequencies and shapes.

Another way to look at this equivalency is as follows. Suppose that the analytical model has an error in it which affects the significant fixed-base modes. Then one would expect that the free-free modes would also be affected by the error, and the free-free model correlation effort would correct the error. The equivalency condition is intended to ensure that there could not be any errors in the model that are significant to the fixed-base modes but "invisible" to the free-free data.

In order to establish equivalence, the test-verified free-free modes were assembled into a dynamic model of the structure. Residual flexibility was included in the free-free representation, even though good agreement was not established. The free-free model was then mathematically constrained at the interface degrees of freedom, and fixed-base natural frequencies and mode shapes were generated. For comparison, the full finite element model was also exercised to predict fixed-base natural frequencies and mode shapes. The predictions of the free-free model and the full model were compared, both for frequency

“ and mode shape, Only the significant fixed base modes (those with effective mass at least 5% of the total mass) were evaluated for this comparison,

The results of this comparison were fairly good. Using the phase 2 configuration, all fixed-base modes below 50 Hz with at least 5% translational effective mass were in agreement within 3% in frequency. Cross orthogonality between the free-free model and the full model was at least 94% for all of these modes except one, where the cross orthogonality was only 62%. This exercise demonstrated that for the significant fixed-base modes, the free-free model is essentially equivalent. Therefore it is unlikely that a model error could remain in the model which would affect the significant fixed-base modes, and not similarly affect the free-free data.

This approach is success oriented. If excellent agreement between the two models can be established, then a strong argument can be made that the fixed-base modes are test-verified. However, results like the 62% cross orthogonality described above are difficult to assess. The modal test community has had so little experience with this type of testing that firm criteria are elusive.

9. CONCLUSIONS

A free-free test with residual flexibility measurement was performed on the SIR-C payload. This test presented many challenges, both experimental and analytical. Not all of the difficulties in this approach were solved.

The following are some of the lessons learned through this experience:

- It is possible to use free-free modes and residual flexibility to verify fixed-base modes of a structure. However, this approach is difficult to implement, and acceptance in the modal test community is slow.
- Extraction of residual flexibility is a difficult process. Few sanity checks are available, and unquantifiable errors can be present in the results. As a result, confidence in the test measurements is low.
- Further research and test cases are needed to develop confidence in the free-free approach. The SIR-C test hopefully provided some forward progress in this area,
- It would be very advantageous to revisit the requirement that the fixed-base modes be accurately predicted by the free-free data. Perhaps a way can be devised to show that the significant in-flight modes are well known.

10. ACKNOWLEDGEMENT

The work described herein was conducted by the Jet Propulsion Laboratory, California Institute of Technology, under contract with National Aeronautics and Space Administration.

11. REFERENCES

- [1] K. Mühlbauer, H. Troidl, S. Dillinger, "Design, Modelling and Verification of a Modal Survey Test Fixture for Space Shuttle Payloads," 10th International Modal Analysis Conference, San Diego, CA, February 1992.
- [2] Admire, J. R., Tinker, M.I., Ivey, E. W., "Mass-Additive Modal Test Method for Verification of Constrained Structural Models," 10th International Modal Analysis Conference, San Diego, CA, February 1992.
- [3] Blair, Mark A., "Space Station Module Prototype Alternative Modal Tests: Fixed Base Alternatives," 11th International Modal Analysis Conference, San Diego, CA, February 1993.
- [4] Blair, Mark A., "Space Station Module Prototype Alternative Modal Tests: Convergence to Fixed Base," 11th International Modal Analysis Conference, San Diego, CA, February 1993.
- [5] Smith, K. S., Peng, C-Y., "SIR-C Antenna Mechanical System Modal Test and Model Correlation Report," Internal Document JPL D-10694, April 20, 1993, Jet Propulsion Laboratory, California Institute of Technology, Pasadena, CA.
- [6] Smith, K. S., "Efficient Updating of Model Parameters Using Modal Coordinates," 12th International Modal Analysis Conference, Honolulu, Hawaii, January 1994.
- [7] Peng, C-Y., Smith, K.S., "Verification of Constrained Shuttle Payloads Using In-Free Modal Test Data: Mathematical Basis" 12th International Modal Analysis Conference, Honolulu, Hawaii, January 1994.

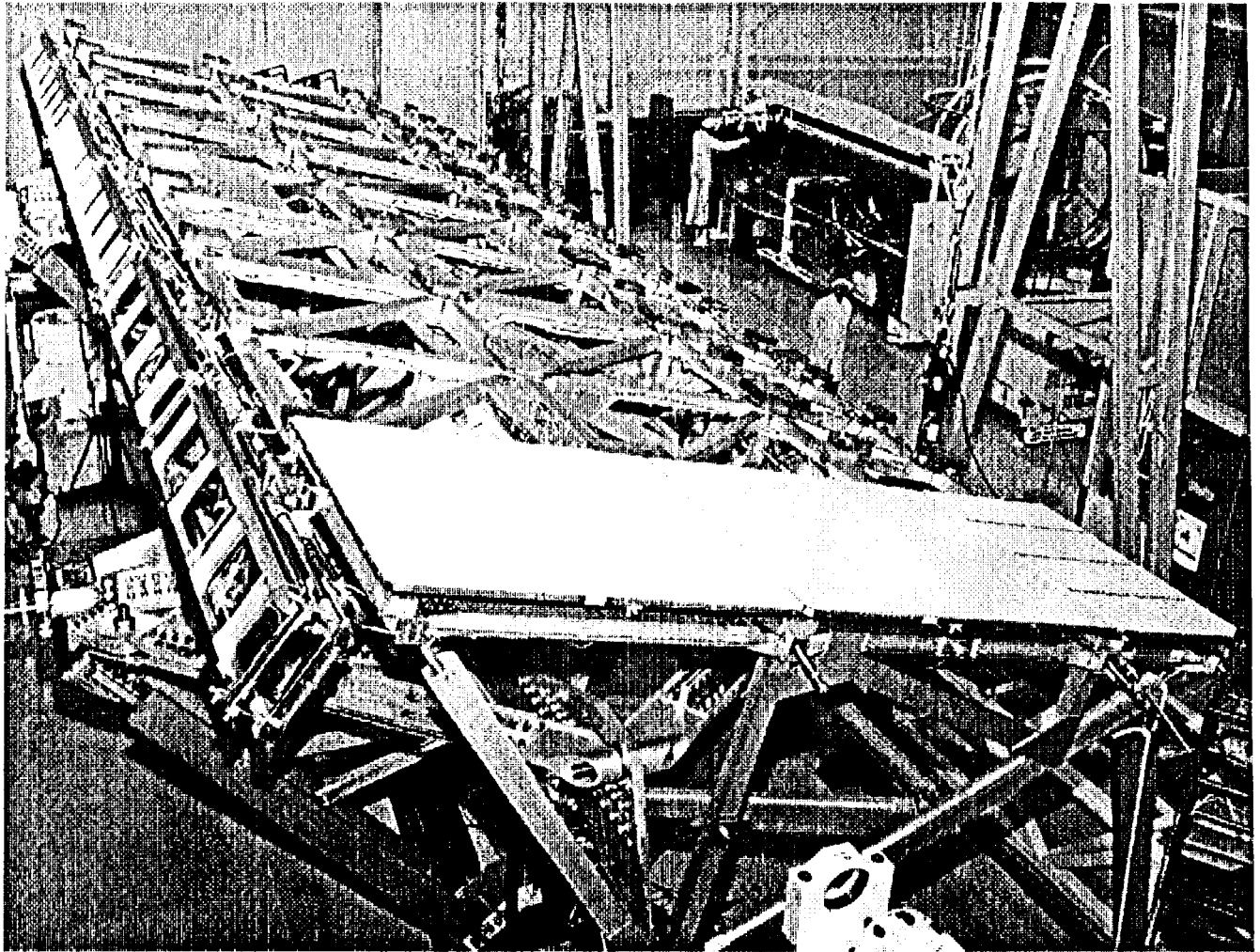


Fig. 2. SIR- C Structure During Modal Test

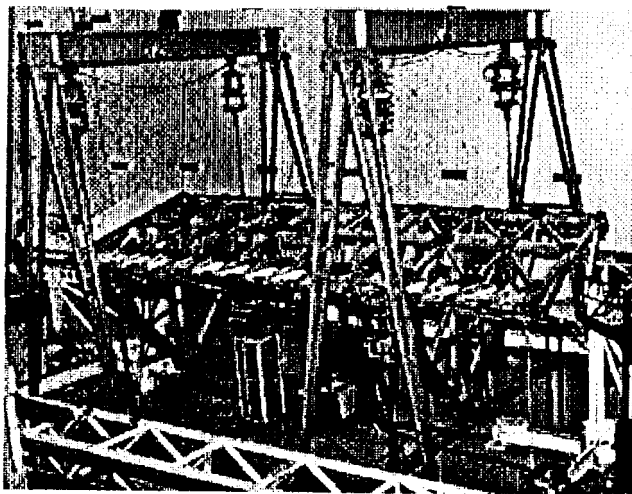


Fig. 3. S1 R- C Structure and Airbag Suspension System

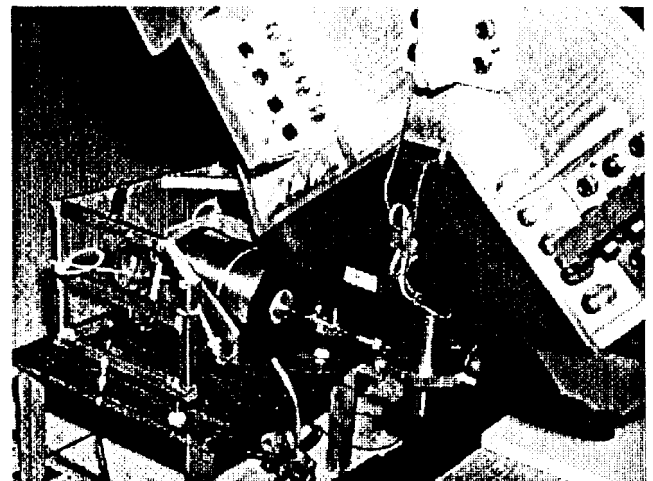


Fig. 4. Typical Shaker Attachment to Trunnion

Table 1. Orthogonality of Test Modes, Phase 1

		Test Modes (Freq in Hz)											
		1	2	3	4	5	6	7	8	9	10	11	
Test Modes (Freq in Hz)	1	5.69											
	2	7.82	3										
	3	17.40	-1	4									
	4	18.54	1	-1	7								
	5	19.17	-1	0	20	8							
	6	19.93	-1	3	9	-2	-8						
	7	21.19	1	6	0	1	7	10					
	8	22.30	0	1	2	-22	-11	-8	20				
	9	22.96	18	-8	3	2	-1	5	-5	-13			
	10	25.40	2	5	-6	-1	4	-6	-4	-2	-9		
	11	26.00	13	-5	-3	1	5	0	-9	-6	-22	-16	

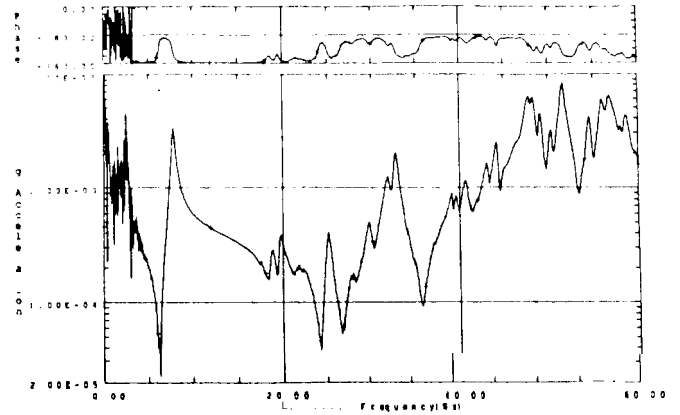


Fig. 6. Example Drive Point FRF Measurement

Table 2. Orthogonality of Test Mods, Phase 2

		Test Modes (Freq in Hz)								
		2	3	4	5	6	7	8	9	
Test Modes (Freq in Hz)	1	5.20								
	2	7.52	-1	0	0	0	-1	2	0	2
	3	11.46	0	0	-9	-1	0	-4	-2	-2
	4	13.73	0	0	-9	7	3	0	2	-3
	5	17.66	0	-2	-1	7	-1	0	-6	-4
	6	17.81	-1	1	0	3	-10	3	1	-3
	7	19.55	2	-4	-4	0	-6	3	16	-5
	8	20.54	0	-4	-2	2	-4	1	1	6
	9	21.61	2	-4	-2	-3	5	-3	-5	-7

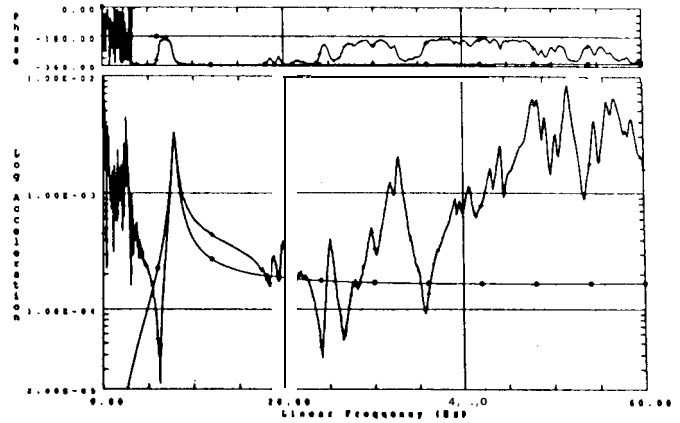


Fig. 7. Curve Fit of 7.8 Hz Mode

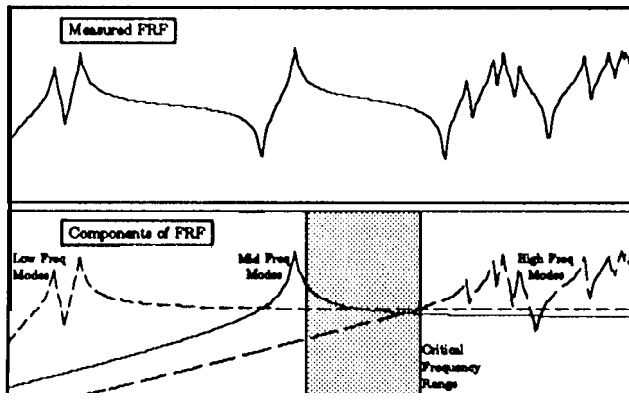


Fig. 5. Schematic Illustration of Residual Flexibility

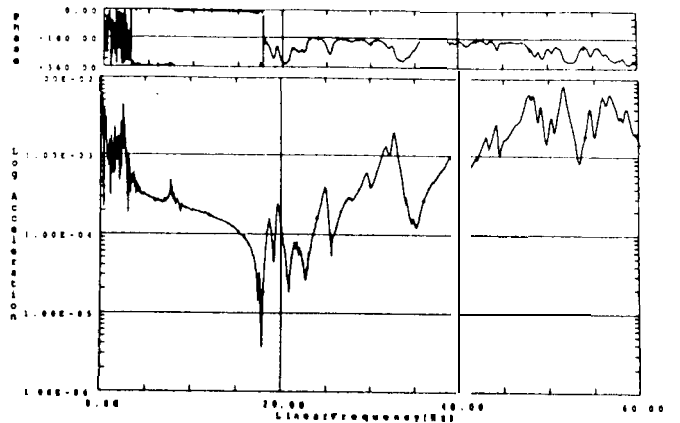


Fig. 8. FRF After Subtraction of 7.8 Hz Curve Fit Mode

Fig. 9. Result After Subtracting Inertance and Dividing by ω^2

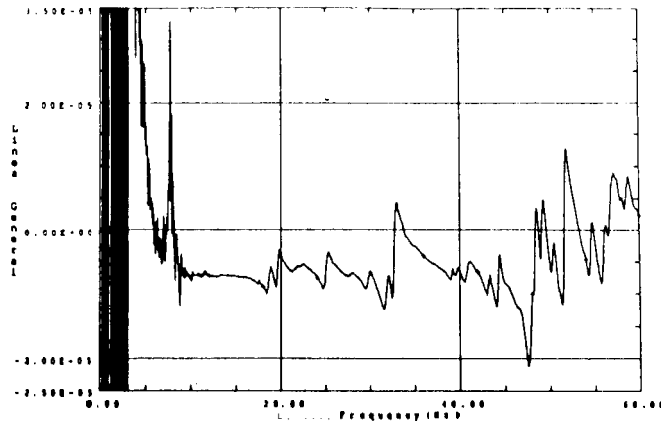


Table 5. Test/Analysis Crow Orthogonality, Phase 1

TAM26 Analysis Modes (Freq in Hz)	Test Modes (Freq in Hz)										
	5.69	7.82	17.40	18.54	19.17	19.93	21.19	22.30	22.96	25.40	26.00
11 3.62	96	1	0	1	-1	0	0	0	10	2	19
12 7.52	3	100	3	-1	0	2	7	1	-8	4	-6
13 16.01	-1	0	89	-12	17	41	-13	15	3	-3	-3
14 18.20	0	0	8	96	5	10	1	-28	4	-7	2
15 18.93	0	0	10	4	92	-4	7	-2	0	-5	4
16 20.02	0	1	32	-7	-16	84	21	-4	3	3	-4
17 21.32	0	-3	4	-1	6	-1	90	10	-7	-15	-8
18 21.67	1	0	-3	5	-11	-3	22	85	-15	-2	-3
19 23.22	1	0	-2	1	0	-1	7	3	92	13	-13
20 23.76	0	1	3	1	11	-3	7	-6	-19	86	-5
21 25.19	1	-1	-18	6	-4	-19	5	21	-9	32	-18
22 26.65	0	-2	4	-3	0	2	3	-9	-2	4	-12
23 26.75	0	0	2	-1	1	0	0	-3	-1	-2	2
24 26.86	-2	0	-2	0	1	1	1	1	-11	-5	89

Table 3. Test/Analysis Frequency Comparison, Phase 1

Test Mode	Freq (Hz)	TAM26 Mode	Freq (Hz)	Freq Error
1	5.69	11	3.62	-36%
2	7.82	12	7.52	-4%
3	17.40	13	16.01	-8%
4	18.54	14	18.20	-2%
5	19.18	15	18.33	-4%
6	19.93	16	20.02	+0%
7	21.19	17	21.32	+1%
8	22.30	18	21.67	-3%
9	22.96	19	23.22	+1%
10	25.40	20	23.76	-6%
		21	25.19	
		22	26.65	
		23	26.75	
11	26.00	24	26.86	+3%

*(frequency of mode 1 not significant for fixed-base modes)

Table 6. Test/Analysis Cross Orthogonality, Phase 2

TAM26 Analysis Modes (Freq in Hz)	Test Modes (Freq in Hz)								
	5.20	7.52	11.46	13.73	17.56	17.81	19.55	20.54	21.62
11 3.61	99	-1	0	0	0	-1	0	-1	2
12 7.36	0	99	0	1	-2	0	-6	-7	-5
13 11.78	0	0	99	-22	-2	-1	-4	-3	-2
14 13.40	0	-1	13	95	3	8	-2	3	-5
15 15.89	-2	1	-1	-2	-8	8	-19	22	3
16 17.96	1	1	0	-7	0	96	-4	3	-3
17 18.38	0	0	1	5	94	-10	-13	-2	6
18 19.61	1	1	0	2	9	7	89	10	10
19 20.54	1	3	0	-1	-1	4	12	91	-1
20 21.09	-1	0	0	1	-1	3	-14	-3	89

Table 4. Test/Analysis Frequency Comparison, Phase 2

Test Mode	Freq (Hz)	TAM26 Mode	Freq (Hz)	Freq Error
1	5.20	11	3.61	-31%
2	7.52	12	7.36	-2%
3	11.46	13	11.78	+3%
4	13.73	14	13.40	-2%
		15	15.89	
5	17.66	17	18.38	+5%
6	17.81	18	17.23	+1%
7	19.55	18	19.61	+0%
8	20.54	19	20.54	+0%
9	21.62	20	21.09	-2%

*(frequency of mode 1 not significant for fixed-base modes)

Table 7. Test/Analysis Residual Flexibility Comparison

	Diagonal Res Flex (in. per million lb)		Ratio TAM/Test
	Test	TAM26	
Woox	53.36	40.82	0.76
Wooz	7.68	4.41	0.57
Wolx	51.69	36.64	0.71
Wolz	13.30	10.06	0.76
W02X	41.11	36.06	0.88
W02Y	9.81	4.66	0.46
9500X	29.26	6.12	0.26
9500Z	5.51	3.93	0.71
9501X	22.65	15.94	0.70
9501Z	12.18	0.11	0.01
9502X	41.01	27.00	0.66
9502Y	7.26	4.49	0.62